J|A|C|S
ARTICLES
Published on Web 07/07/2006

Conversion of Methane to Methanol at the Mononuclear and Dinuclear Copper Sites of Particulate Methane Monooxygenase (pMMO): A DFT and QM/MM Study

Kazunari Yoshizawa* and Yoshihito Shiota

Contribution from the Institute for Materials Chemistry and Engineering, Kyushu University, Fukuoka 812-8581, Japan

Received March 16, 2006; E-mail: kazunari@ms.ifoc.kyushu-u.ac.jp

Abstract: Methane hydroxylation at the mononuclear and dinuclear copper sites of pMMO is discussed using quantum mechanical and QM/MM calculations. Possible mechanisms are proposed with respect to the formation of reactive copper−oxo and how they activate methane. Dioxygen is incorporated into the Cu^{I} species to give a Cu^{II}−superoxo species, followed by an H-atom transfer from a tyrosine residue near the monocopper active site. A resultant Cu^{II}−hydroperoxo species is next transformed into a Cu^{III}−oxo species and a water molecule by the abstraction of an H-atom from another tyrosine residue. This process is accessible in energy under physiological conditions. Dioxygen is also incorporated into the dicopper site to form a (μ-η^2:η^2-peroxo)dicopper species, which is then transformed into a bis(μ-oxo)dicopper species. The formation of this species is more favorable in energy than that of the monocopper−oxo species. The reactivity of the Cu^{III}−oxo species is sufficient for the conversion of methane to methanol if it is formed in the protein environment. Since the σ^* orbital localized in the Cu−O bond region is singly occupied in the triplet state, this orbital plays a role in the homolytic cleavage of a C−H bond of methane. The reactivity of the bis(μ-oxo)dicopper species is also sufficient for the conversion of methane to methanol. The mixed-valent bis(μ-oxo)$Cu^{II}Cu^{III}$ species is reactive to methane because the amplitude of the σ^* singly occupied MO localized on the bridging oxo moieties plays an essential role in C−H activation.

Introduction

Methanotrophic bacteria oxidize methane using molecular dioxygen to form methanol, formaldehyde, formic acid, and finally carbon dioxide.[1] In the initial stages of the methane oxidation pathway, the inert alkane is efficiently converted into methanol by methane monooxygenase (MMO) under physiological conditions. This initial methane oxidation is conducted by methanotrophs such as *Methylococcus capsulatus* (Bath) and *Methylosinus trichosporium* OB3b. In both species of methanotrophs two different forms are known to exist under different conditions, a cytoplasmic (soluble) MMO and a membrane-bound (particulate) MMO. Particulate MMO (pMMO) is a copper-containing membrane protein,[2,3] but in contrast to soluble MMO (sMMO) the structure of the pMMO active site remained unknown because of the difficulty in handling the purified pMMO. Methane oxidation is carried out mostly by sMMO under conditions of copper limitation. Different mechanisms on the hydroxylation of methane at the diiron active site of sMMO were proposed on the basis of quantum chemical computations.[4−7] However, addition of copper to the growth medium significantly increases the activity of pMMO. Thus, although the role of copper in the pMMO activity is not fully understood, copper may play an essential role in the methane oxidation by pMMO.

The structure of pMMO, recently determined to a resolution of 2.8 Å (Protein Data Bank code 1YEW), reveals a trimeric arrangement and overall folds of the three subunits.[8] There are three metal centers per protomer in the crystal structure. Two of these, which were modeled as mononuclear and dinuclear

(1) (a) Feig, A. L.; Lippard, S. J. *Chem. Rev.* **1994**, *94*, 759. (b) Lipscomb, J. D. *Annu. Rev. Microbiol.* **1994**, *48*, 371. (c) Wallar, B. J.; Lipscomb, J. D. *Chem. Rev.* **1996**, *96*, 2625. (d) Que, L., Jr.; Dong, Y. *Acc. Chem. Res.* **1996**, *29*, 190. (e) Merkx, M.; Kopp, D. A.; Sazinsky, M. H.; Blazyk, J. L.; Müller, J.; Lippard, S. J. *Angew. Chem., Int. Ed.* **2001**, *40*, 2782.
(2) Chan, S. I.; Chen, K. H.-C.; Yu, S. S.-F.; Chen, C.-Li.; Kuo, S. S.-J. *Biochemistry* **2004**, 43, 4421.
(3) Lieberman, R. L.; Shrestha, D. B.; Doan, P. E.; Hoffman, B. M.; Stemmler, T. L.; Rosenzeig, A. C. *Proc. Natl. Acad. Sci. U.S.A.* **2003**, *100*, 3820.
(4) (a) Yoshizawa, K.; Yamabe, T.; Hoffmann, R. *New J. Chem.* **1997**, *21*, 151. (b) Yoshizawa, K.; Ohta, T.; Yamabe, T.; Hoffmann, R. *J. Am. Chem. Soc.* **1997**, *119*, 12311. (c) Yoshizawa, K. *J. Biol. Inorg. Chem.* **1998**, *3*, 318. (d) Yoshizawa, K.; Ohta, T.; Yamabe, T. *Bull. Chem. Soc. Jpn.* **1998**, *71*, 1899. (e) Yoshizawa, K.; Suzuki, A.; Shiota, Y.; Yamabe, T. *Bull. Chem. Soc. Jpn.* **2000**, *73*, 815. (f) Yoshizawa, K. *J. Inorg. Biochem.* **2000**, *78*, 23. (g) Yoshizawa, K.; Yumura, T. *Chem. Eur. J.* **2003**, *9*, 2347.
(5) (a) Siegbahn, P. E. M.; Crabtree, R. H. *J. Am. Chem. Soc.* **1997**, *119*, 3103. (b) Siegbahn, P. E. M.; Crabtree, R. H.; Nordlund, P. *J. Biol. Inorg. Chem.* **1998**, *3*, 314. (c) Siegbahn, P. E. M. *Inorg. Chem.* **1999**, *38*, 2880. (d) Siegbahn, P. E. M.; Blomberg, M. R. A. *Chem. Rev.* **2000**, *100*, 421. (e) Siegbahn, P. E. M. *J. Biol. Inorg. Chem.* **2001**, *6*, 27.
(6) (a) Basch, H.; Mogi, K.; Musaev, D. G.; Morokuma, K. *J. Am. Chem. Soc.* **1999**, *121*, 7249. (b) Basch, H.; Musaev, D. G.; Mogi, K.; Morokuma, K. *J. Phys. Chem. A* **2001**, *105*, 3615. (c) Basch, H.; Musaev, D. G.; Morokuma, K. *J. Phys. Chem. B* **2001**, *105*, 8452. (d) Torrent, M.; Musaev, D. G.; Basch, H.; Morokuma, K. *J. Comput. Chem.* **2002**, *23*, 59.
(7) (a) Dunietz, B. D.; Beachy, M. D.; Cao, Y.; Whittington, D. A.; Lippard, S. J.; Friesner, R. A. *J. Am. Chem. Soc.* **2000**, *122*, 2828. (b) Gherman, B. F.; Dunietz, B. D.; Whittington, D. A.; Lippard, S. J.; Friesner, R. A. *J. Am. Chem. Soc.* **2001**, *123*, 3836. (c) Guallar, V.; Gherman, B. F.; Miller, W. H.; Lippard, S. J.; Friesner, R. A. *J. Am. Chem. Soc.* **2002**, *124*, 3377. (d) Baik, M.-H., Newcomb, M.; Friesner, R. A.; Lippard, S. J. *Chem. Rev.* **2003**, *103*, 2385.
(8) Lieberman, R. L.; Rosenzweig, A. C. *Nature* **2005**, *434*, 177.

copper species, are located within the soluble regions of the pmoB subunit, the two copper sites being 21 Å apart from each other. The third metal center, which is occupied by zinc in the crystal, lies within the membrane with ligands derived from both pmoC and pmoA. It is 19 Å apart from the dicopper site and 32 Å apart from the monocopper site. The zinc is derived from crystallization buffer, and its site is probably occupied by another metal ion in vivo such as copper or iron.

Earlier proposals for the structure of the pMMO active site include mixed-valent trinuclear Cu^{II},[9] mononuclear Cu^{II},[10−14] dinuclear mixed-valent $Cu^{II}Cu^{III}$ clusters,[15] and mixed-metal CuFe clusters.[16] The di-μ-oxo dicopper structure has been proposed from model-complex studies to be responsible for dioxygen activation and hydrocarbon oxidation.[17−19] A recent DFT study demonstrated that a bis(μ_3-oxo)trinuclear $Cu^{II}Cu^{II}$-Cu^{III} model can best mediate methane hydroxylation via a concerted oxo-insertion manner.[20] However, since such a trinuclear copper site is not found in the crystal structure of pMMO, we restrict our discussion to the reactivity of the observed monocopper and dicopper species. In a previous density functional theory (DFT) study[21] we proposed a mechanism for the C−H cleavage and the recombination between CH_3 and OH ligands using a simple mixed-valent dinuclear $Cu^{II}Cu^{III}$ cluster with ammonia and hydroxo ligands. On the basis of the recent crystal structure of pMMO,[8] it is possible to derive much better results using more realistic copper-active species. In this manuscript we report a new study on the mechanism of methane hydroxylation at the mononuclear and dinuclear copper sites on the basis of the crystal structure of pMMO and consider how reactive copper species are formed in the protein environment.

Method of Calculation

In this study we assumed that two kinds of copper−oxo species formed at the mononuclear and dinuclear copper sites play an essential role in the conversion of methane to methanol. It is found from the X-ray structural analysis[4] that Glu75 and Glu35 are located near the monocopper and dicopper sites, respectively. On the basis of this observation, we set up a Cu^{III}−oxo (or Cu^{II}−$O^{\bullet}$) model in which the copper ion is coordinated by His48, His72, and Glu75 and a mixed-valent bis(μ-oxo)$Cu^{II}Cu^{III}$ model in which the two copper ions are coordinated by His33, His137, His139, and Glu35. Although it is difficult to set up their charge states, we adopted this assumption because one glutamate ligand is located in the neighborhood of both the mononuclear and dinuclear copper sites. Each model is neutral in its charge owing to a negatively charged glutamate ligand. The three-dimensional models for the monomeric structure of pMMO (about 6000 atoms) were optimized with the two-layer ONIOM (IMOMM) method,[22] implemented in the Gaussian 03 program.[23] In these quantum mechanical/molecular mechanical (QM/MM) calculations, a specified region around the active center was calculated with a QM method, while the rest of the protein was treated at an MM level. The QM region can describe the essential bond-cleaving and bond-forming processes in the enzyme, while the MM region can promote interactions with the QM region through partial charges and van der Waals forces of atoms in the MM region. At the QM/MM border, atoms in the MM region bound to an atom in the QM region were replaced by hydrogen atoms in the QM-level part of the QM/MM calculation. The QM region includes the mononuclear and dinuclear copper sites and their surrounding amino acid residues. QM calculations were performed with the B3LYP* method,[24] which consists of the Slater exchange, the Hartree−Fock exchange, the exchange functional of Becke,[25] the correlation functional of Lee, Yang, and Parr (LYP),[26] and the correlation functional of Vosko, Wilk, and Nusair.[27] This DFT method is an improved version of B3LYP and able to reasonably evaluate relative energies between high-spin and low-spin states of transition-metal complexes in general. We used the Wachters−Hay basis set[28] for the copper atoms and the D95** basis set[29] for the surrounding amino acid residues. The method of choice for MM calculations is the Amber force field (Amber96).[30]

We looked at the energy profiles for the C−H bond cleavage and oxygen rebound process in the hydroxylation of methane using small models extracted from the QM region of the QM/MM optimized structures. All the geometries for the reaction species and transition states were fully optimized without symmetry constraint at the same level of theory. The spin-unrestricted version of the B3LYP* (UB3LYP*) method was applied to all calculations including spin-singlet states when the reaction species are reasonably considered to have an open-shell-singlet electronic configuration. We performed vibrational analyses for all transition states to confirm whether an optimized geometry corresponds to a transition state that has only one imaginary frequency. Kinetic isotope effect (KIE) values in the H-atom abstraction were calculated in a wide range of temperature from transition state theory[31] with Wigner's tunneling correction.[32]

(9) (a) Nguyen, H.-H. T.; Shiemke, A. K.; Jacobs, S. J.; Hales, B. J.; Lidstrom, M. E.; Chan, S. I. *J. Biol. Chem.* **1994**, *269*, 14995. (b) Nguyen, H.-H. T.; Nakagawa, K. H.; Hedman, B.; Elliott, S. J.; Lidstrom, M. E.; Hodgson, K. O.; Chan, S. I. *J. Am. Chem. Soc.* **1996**, *118*, 12766.
(10) Yuan, H.; Collins, M. L. P.; Antholine, W. E. *J. Am. Chem. Soc.* **1997**, *119*, 5073.
(11) Takeguchi, M.; Miyakawa, K.; Okura, I. *J. Mol. Catal. A* **1998**, *132*, 145.
(12) Lemos, S. S.; Yuan, H.; Perille-Collins, M. L. *Curr. Top. Biophys.* **2002**, *26*, 43.
(13) Choi, D. W.; Kunz, R. C.; Boyd, E. S.; Semrau, J. D. *J. Bacteriol.* **2003**, *185*, 5755.
(14) Basu, P.; Katterle, B.; Andersson, K. K.; Dalton, H. *Biochem. J.* **2003**, *369*, 417.
(15) Elliott, S. J.; Zhu, M.; Tso, L.; Nguyen, H.-H. T.; Yip, J. H.-K.; Chan, S. I. *J. Am. Chem. Soc.* **1997**, *119*, 9949.
(16) (a) Zhan, J. A.; DiSpirito, A. A. *J. Bacteriol.* **1996**, *178*, 1018. (b) Kim, H. J.; Graham, D. W.; DiSpirito, A. A.; Alterman, M. A.; Galeva, N.; Larive, C. K.; Asunskis, D.; Sherwood, P. A. M. *Science* **2004**, *305*, 1612.
(17) (a) Pidcock, E.; Obias, H. V.; Zhang, X.; Karlin, K. D.; Solomon, E. I. *J. Am. Chem. Soc.* **1998**, *120*, 7841. (b) Obias, H. V.; Lin, Y.; Murthy, N. N.; Pidcock, E.; Solomon, E. I.; Ralle, M.; Blackburn, N. J.; Neuhold, Y.-M.; Zuberbühler, A. D.; Karlin, K. D. *J. Am. Chem. Soc.* **1998**, *120*, 12960.
(18) (a) Halfen, J. A.; Mahapatra, S.; Wilkinson, E. C.; Kaderli, S.; Young, V. G., Jr.; Que, L., Jr.; Zuberbüler, A. D.; Tolman, W. B. *Science* **1996**, *271*, 1397. (b) Mahapatra, S.; Halfen, J. A.; Wilkinson, E. C.; Pan, G.; Wang, X.; Young, V. G., Jr.; Cramer, C. J.; Que, L., Jr.; Tolman, W. B. *J. Am. Chem. Soc.* **1996**, *118*, 11555. (c) Mahapatra, S.; Young, V. G., Jr.; Kaderli, S.; Zuberbüler, A. D.; Tolman, W. B. *Angew. Chem., Int. Ed.* **1997**, *36*, 130.
(19) (a) Itoh, S.; Nakao, H.; Berreau, L. M.; Kondo, T.; Komatsu, M.; Fukuzumi, S. *J. Am. Chem. Soc.* **1998**, *120*, 2890. (b) Taki, M.; Itoh, S.; Fukuzumi, S. *J. Am. Chem. Soc.* **2001**, *123*, 6203.
(20) Chen, P. P.-Y.; Chan, S. I. *J. Inorg. Biochem.* **2006**, *100*, 801.
(21) Yoshizawa, K.; Suzuki, A.; Shiota, Y.; Yamabe, T. *Bull. Chem. Soc. Jpn.* **2000**, *73*, 815.
(22) (a) Maseras, F.; Morokuma, K. *J. Comput. Chem.* **1995**, *16*, 1170. (b) Svensson, M.; Humbel, S.; Froese, R. D. J.; Matsubara, T.; Sieber, S.; Morokuma, K. *J. Phys. Chem.* **1996**, *100*, 19357. (c) Vreven, T.; Morokuma, K. *J. Comput. Chem.* **2000**, *21*, 1419.
(23) Frisch, M. J.; et al. *Gaussian 03*; Gaussian, Inc.: Wallingford, CT, 2004.
(24) (a) Reiher, M.; Salomon, O.; Hess, B. A. *Theor. Chem. Acc.* **2001**, *107*, 48. (b) Reiher, M.; Salomon, O.; Hess, B. A. *J. Chem. Phys.* **2002**, *117*, 4729.
(25) (a) Becke, A. D. *Phys. Rev. A* **1988**, *38*, 3098. (b) Becke, A. D. *J. Chem. Phys.* **1993**, *98*, 5648.
(26) Lee, C.; Yang, W.; Parr, R. G. *Phys. Rev. B* **1988**, *37*, 785.
(27) Vosko, S. H.; Wilk, L.; Nusair, M. *Can. J. Phys.* **1980**, *58*, 1200.
(28) (a) Wachters, A. J. H. *J. Chem. Phys.* **1970**, *52*, 1033. (b) Hay, P. J. *J. Chem. Phys.* **1977**, *66*, 4377.
(29) Dunning, T. H.; Hay, P. J. In *Modern Theoretical Chemistry*; Schaefer, H. F., III, Ed.; Plenum: New York, 1976; Vol. 3, p 1.
(30) Cornell, W. D.; Cieplak, P.; Bayly, C. I.; Gould, I. R.; Merz, K. M., Jr.; Ferguson, D. M.; Spellmeyer, D. C.; Fox, T.; Caldwell, J. W.; Kollman, P. A. *J. Am. Chem. Soc.* **1995**, *117*, 5179.
(31) Frost, A. A.; Pearson, R. G. *Kinetics and Mechanism*; Wiley: New York, 1961.
(32) Wigner, E. *J. Chem. Phys.* **1937**, **5**, 720.

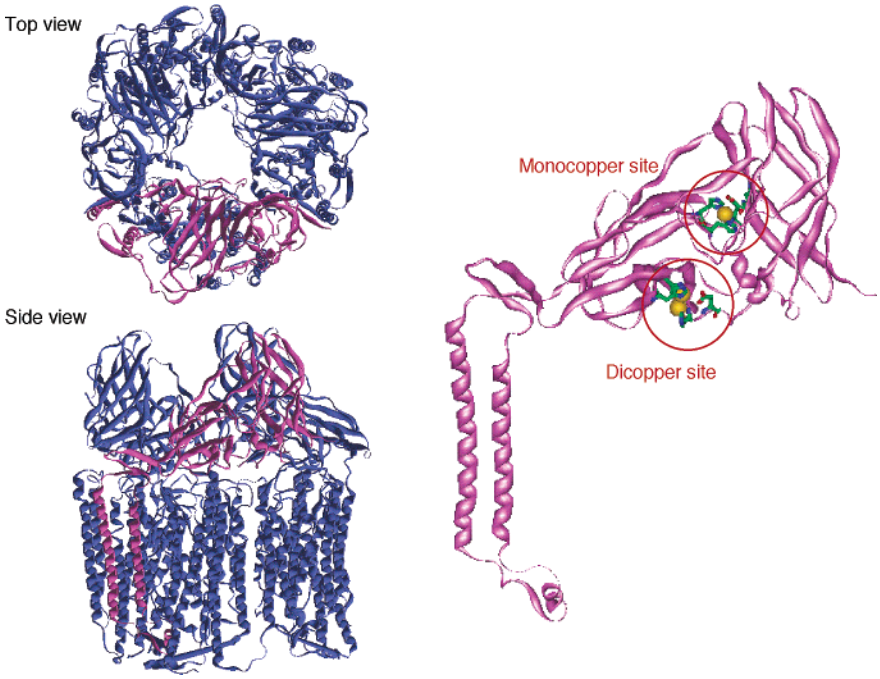

Figure 1. X-ray structure of the pMMO trimer (left) and QM/MM-optimized structure of the protomer (right).

Results and Discussion

QM/MM Structures of the Copper Sites of pMMO. Figure 1 (left) shows the top and side views of the trimeric structure of pMMO determined at 2.8 Å resolution.[8] Each protomer in the trimeric structure is composed of three subunits; pmoB (~47 kDa), pmoA (~24 kDa), and pmoC (~22 kDa). In the present study we turned our attention to a pmoB unit that includes the mononuclear and dinuclear copper sites and optimized its geometry using QM/MM calculations. Figure 1 (right) is a QM/MM optimized structure of the pmoB. Detailed geometrical information can be seen in Supporting Information.

Let us now look at the copper active sites in pmoB in detail. The mononuclear copper center is directly coordinated by His48 and His72, as shown in Figure 2a. Although Gln404 and Glu75 are located in the vicinity of this site, the copper ion takes a two-coordination structure. The formal charge of the mononuclear species is reasonably counted to be +1, and therefore the ground state of this species is a spin singlet. The dinuclear copper site, which is coordinated by His33, His137, His139, and Glu35 has a short Cu−Cu bond of 2.474 Å, as shown in Figure 2b. Since the Glu35 residue is located near this dinuclear site and as a result the formal charge of the dinuclear species is also counted to be +1, its ground state is a spin doublet. The QM/MM optimized Cu−Cu distance is in good agreement with 2.6 Å determined by EXAFS and X-ray structural analyses.[3,8] Thus, the optimized structures of the resting mononuclear and dinuclear copper sites are consistent with the X-ray structure with respect to their coordination spheres. The intermolecular $d^{10}-d^{10}$ interaction detected in a large number of crystal structures is a recent interest for computational quantum chemistry. This dispersion interaction is correctly treated by second-order perturbation computations whereas the shape and stability of the $d^{10}-d^{10}$ interaction curves derived from perturbation computations are roughly reproduced by B3LYP computations.[33] We thus used the B3LYP method throughout the present study, considering the sizes of the QM/MM and cluster models adopted.

We assumed that two kinds of copper−oxo species are formed at the mononuclear and dinuclear copper sites for methane activation. QM/MM calculations tell us that the mononuclear copper−oxo species is coordinated by His48, His72, and Glu75, as demonstrated in Figure 2c. The negatively charged Glu75 residue directly coordinates to the copper ion, the formal charge of which is +3, whereas the neutral Gln404 residue has no direct interaction with the copper ion. This coordination environment is reasonable from the point of view of electrostatic interactions. The interacting Cu−O(Glu75) bond is optimized to be 2.197 Å. The dinuclear copper site is coordinated by His33, His137, His139, and Glu35, as shown in Figure 2d. Although both the N-terminal amino nitrogen and the side-chain δ nitrogen of His33 are within coordinating distance to the right-side copper ion in the resting state, as indicated in Figure 2b, the negatively charged Glu35 residue directly coordinates to this copper ion in the dicopper−oxo species. The Cu−O(Glu35) distance is optimized to be 1.972 Å. This geometrical change in the coordination environment can also be derived from electrostatic interactions. The formal charge of the left-side copper ion is reasonably counted to be +2 and that of the right-side copper ion +3, and therefore this is a mixed-valent bis(μ-oxo)$Cu^{II}Cu^{III}$ structure, in which the Cu−Cu distance is optimized to be 2.757 Å. Thus, the glutamate residues play an important role in the compensation of electric charges after the formation of the copper−oxo species.

Methane Hydroxylation Mechanism. By looking at the coordination environments of the QM/MM-optimized monocopper− and dicopper−oxo species, we set up two kinds of model complexes for DFT calculations to search the reaction pathway for the conversion of methane to methanol. One is a $Cu^{III}-O$ (or $Cu^{II}-O^{\bullet}$) model with two imidazoles and one acetate, and the other is a mixed-valent bis(μ-oxo)$Cu^{II}Cu^{III}$

(33) Carvajal, M. A.; Alvarez, S.; Novoa, J. J. *Chem. Eur. J.* **2004**, *10*, 2117.

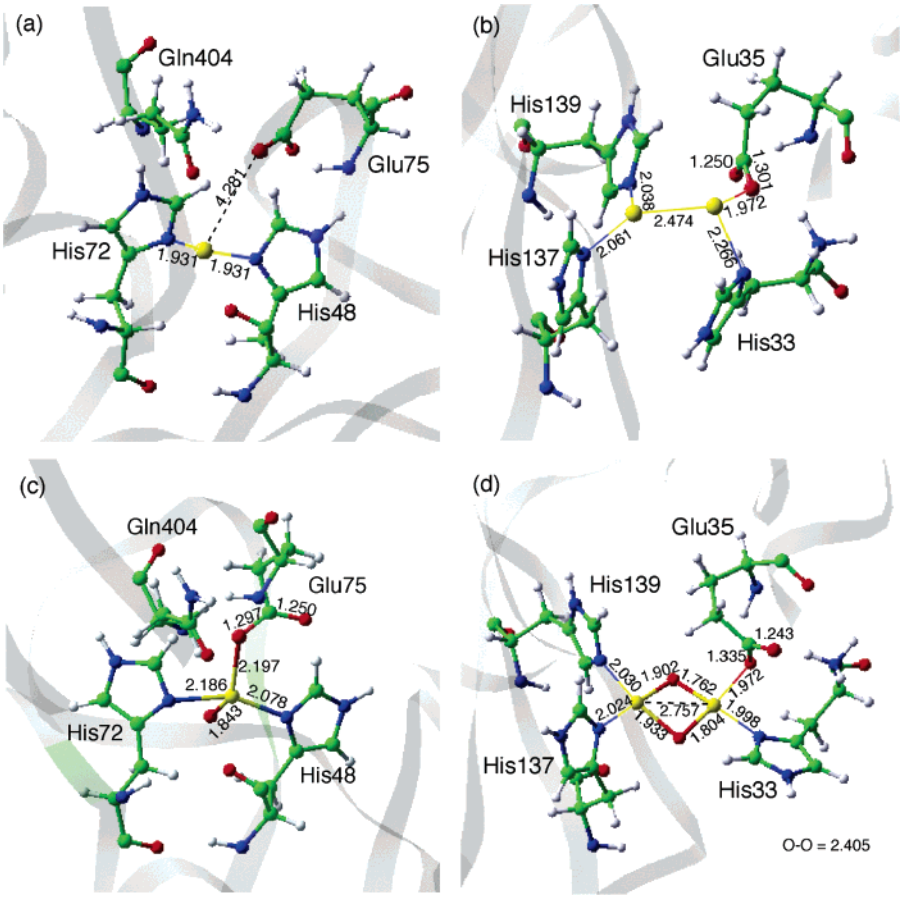

Figure 2. QM/MM-optimized structures for (a) the monocopper site, (b) the dicopper site, (c) the monocopper−oxo species, and (d) the bis(μ-oxo)$Cu^{II}Cu^{III}$ species of pMMO.

model with three imidazoles and one acetate. We characterized reaction intermediates and transition states involved in the reaction pathway from methane to methanol using these relatively small models at the B3LYP* level of theory.

Figure 3 shows computed energy diagrams for methane hydroxylation by the monocopper−oxo species, in which both the singlet and triplet potential energy surfaces are close-lying in energy.The copper−oxo species (**Oxo(m)**) optimized using a small model in the gas phase is in good agreement with the one optimized in the protein environment (shown in Figure 2) with respect to the coordination bonds around the central copper atom. In the initial stages of the reaction, methane is weakly bound to the monocopper active center (**R(m)**), and after that, one of the C−H bonds of methane is cleaved by the oxo species via the first transition state (**TS1(m)**). The activation energy in this process is computed to be 16.6 kcal/mol relative to the dissociation limit on the triplet potential energy surface. The resultant radical species (**Rad(m)**) leads to a nonradical intermediate (**Int(m)**), which is extremely stable in energy in the singlet state. Since the formal charge of the copper ion is changed from +3 to +1 after the H-atom abstraction, this result is reasonable. The second transition state (**TS2(m)**), which has a typical triangular structure for the recombination between the OH and CH_3 ligands, is low in reactivity in comparison with that of the first one. Therefore the rate-determining step of the reaction pathway is clearly in the H-atom abstraction step. The formation of the product (**P(m)**) is computed to be 52.9 kcal/mol exothermic relative to the formation of the monocopper−oxo species + CH_4. The triplet state plays a more important role in the first half of the reaction, whereas the singlet state is dominant in the second half of the reaction. Therefore, we expect that the spin inversion from triplet to singlet should take place in the course of this reaction (near the H-atom abstraction step). This is a typical example of the two-state-reactivity concept.[34] Spin−orbit coupling is an important factor in determining spin inversion electronic processes in transition-metal-mediated reactions and spin-crossover phenomena.[35] The general features of this reaction are similar to those of methane hydroxylation by the bare CuO^+ complex[36] and of dopamine hydroxylation by a possible copper−oxo species of dopamine β-monooxygenase.[37]

The high reactivity of the mononuclear Cu^{III}−oxo species to methane especially in the triplet state is rationalized from the singly occupied molecular orbitals (SOMOs) shown in Figure 4. Since the σ^* orbital partially localized in the Cu−O bond region (orbital #71) is half occupied in the triplet state, this orbital plays a crucial role in the homolytic cleavage of a C−H bond of methane. On the other hand, in the singlet-state orbital #71 is vacant while orbital #70 is occupied by two electrons.

(34) (a) Fiedler, A.; Schröder, D.; Shaik, S.; Schwarz, H. *J. Am. Chem. Soc.* **1994**, *116*, 10734. (b) Shaik, S.; Danovich, D.; Fiedler, A.; Schröder, D.; Schwarz, H. *Helv. Chim. Acta* **1995**, *78*, 1393. (c) Schröder, D.; Shaik, S.; Schwarz, H. *Acc. Chem. Res.* **2000**, *33*, 139.
(35) (a) Shiota, Y.; Yoshizawa, K. *J. Chem. Phys.* **2003**, *118*, 5872. (b) Kondo, M.; Yoshizawa, K. *Chem. Phys. Lett.* **2003**, *372*, 519.
(36) (a) Yoshizawa, K.; Shiota, Y.; Yamabe, T. *Chem. Eur. J.* **1997**, *3*, 1160. (b) Yoshizawa, K.; Shiota, Y.; Yamabe, T. *J. Am. Chem. Soc.* **1998**, *120*, 564. (c) Shiota, Y.; Yoshizawa, K. *J. Am. Chem. Soc.* **2000**, *122*, 12317.
(37) (a) Kamachi, T.; Kihara, N.; Shiota, Y.; Yoshizawa, K. *Inorg. Chem.* **2005**, *44*, 4226. (b) Yoshizawa, K.; Kihara, N.; Kamachi, T.; Shiota, Y. *Inorg. Chem.* **2006**, *45*, 3034.

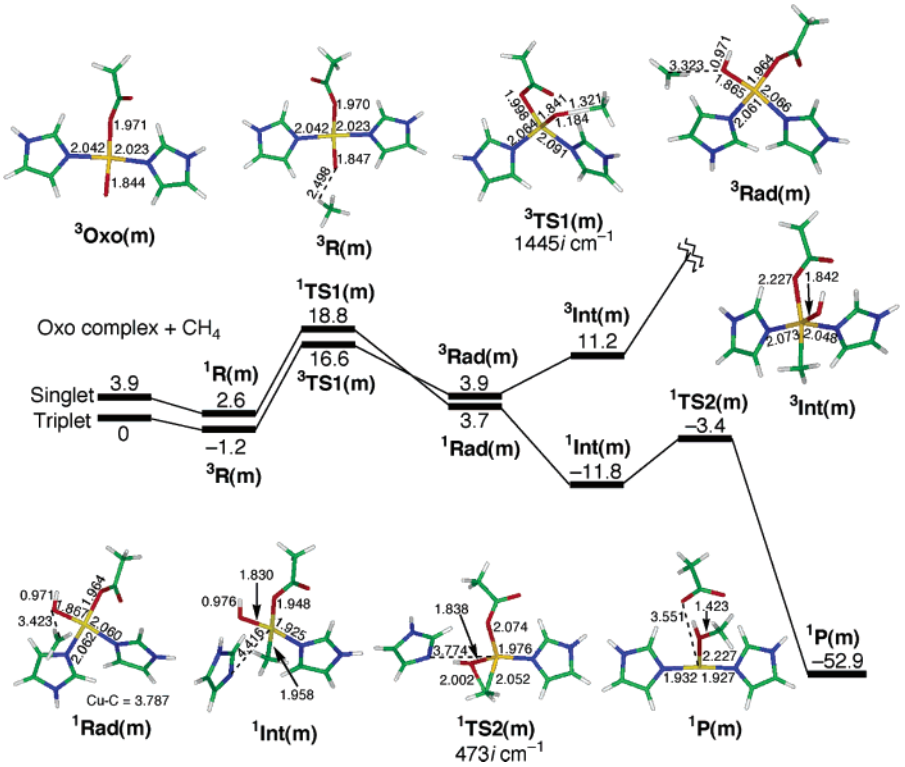

Figure 3. Energy diagram for the conversion of methane to methanol by the monocopper−oxo species of pMMO. Units in kcal/mol.

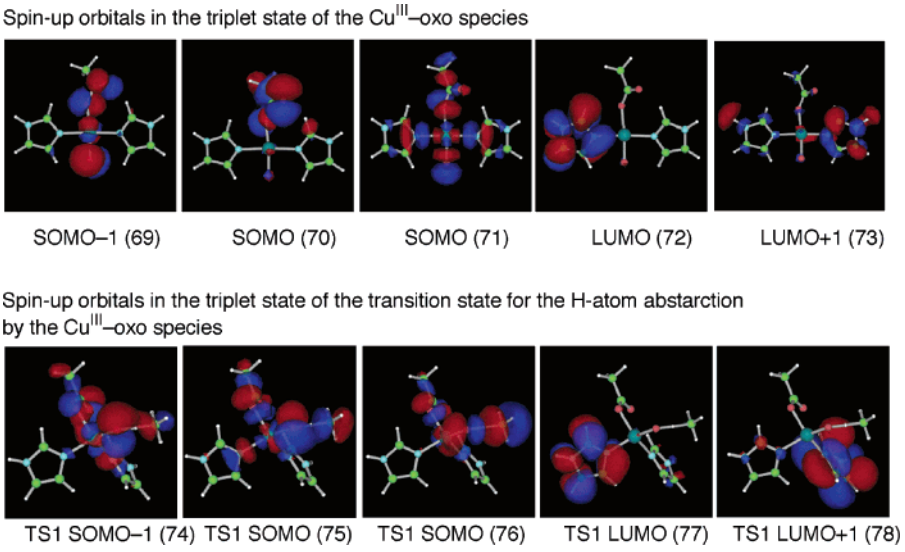

Figure 4. Frontier molecular orbitals for the monocopper−oxo species and the transition state for the H-atom abstraction.

As a consequence, the reactivity of the mononuclear Cu^{III}−oxo species in the singlet state is lower than that in the triplet state. This qualitative observation of the frontier orbitals well explains the computational result shown in Figure 3 on the general features on the reactivity of the Cu^{III}−oxo species to methane.

A computed energy diagram for methane hydroxylation by the mixed-valent bis(μ-oxo)$Cu^{II}Cu^{III}$ species is shown in Figure 5, in which the doublet potential energy surface plays an essential role, whereas the quartet potential energy surface in the dicopper species is high-lying in energy. The mechanism is similar to the one by the Cu^{III}−oxo species. The dicopper−oxo species (**Oxo(d)**) optimized using a small model agrees well with the one optimized in the protein environment (shown in Figure 2) about the coordination bonds around the two copper atoms. Methane is weakly bound to the right-side copper center of the dicopper species (**R(d)**), and after that H-atom abstraction from the methane takes place via **TS1(d)**. The activation energy in this process is computed to be 17.6 kcal/mol relative to the dissociation limit on the doublet potential energy surface. The resultant methyl radical (**Rad(d)**) is also trapped at the right-side copper center to form a nonradical intermediate (**Int(d)**). Since methyl radical is very unstable compared to other alkyl radicals, the formation of this nonradical species is reasonable from the viewpoint of energy. The final step is a recombination between the OH ligand located at the left-side copper center and the CH_3 ligand located at the right-side copper center via **TS2(d)**, which is computed to be 21.5 kcal/mol relative to the

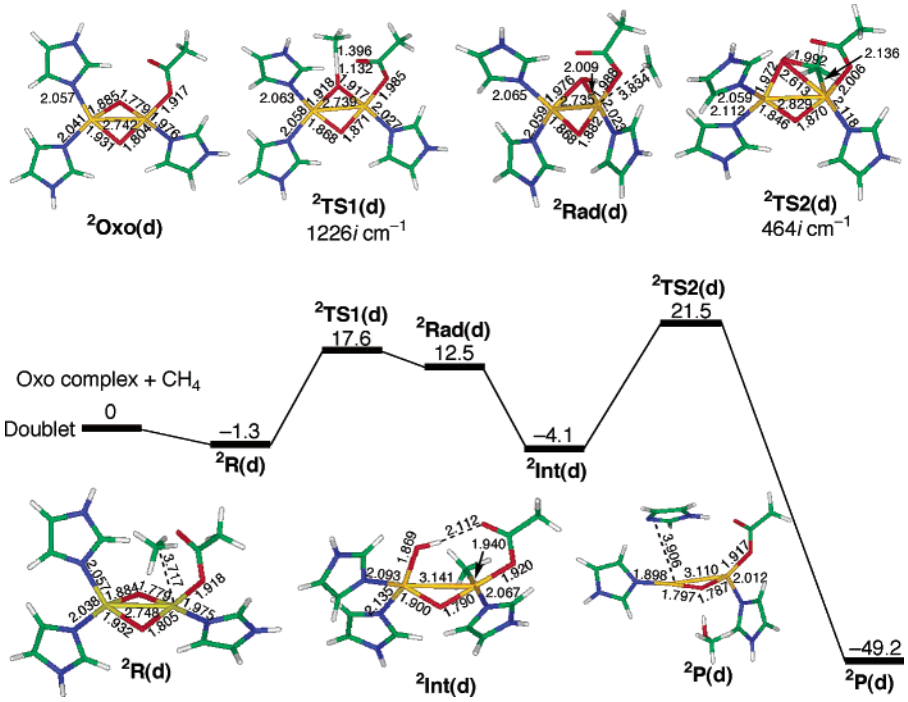

Figure 5. Energy diagram for the conversion of methane to methanol by the bis(μ-oxo)Cu^{II}Cu^{III} species of pMMO. Units in kcal/mol.

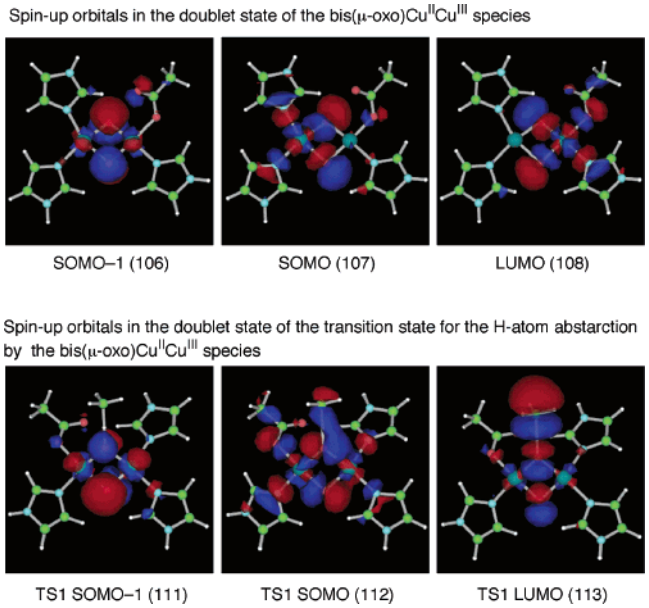

Figure 6. Frontier molecular orbitals for bis(μ-oxo)Cu^{II}Cu^{III} species of pMMO and the transition state for the H-atom abstraction.

dissociation limit. Therefore the rate-determining step of the reaction pathway is the recombination step. The formation of the product (**P(d)**) is computed to be 49.2 kcal/mol exothermic relative to the formation of the dicopper−oxo species + CH_4.

The high reactivity of the mixed-valent bis(μ-oxo)Cu^{II}Cu^{III} species is reasonable in view of the SOMO (orbital #107) shown in Figure 6. Since the amplitude of this σ* SOMO is localized well on the bridging oxo moieties, this orbital works as a good mediator in the homolytic C−H cleavage of methane. On the other hand, in the bis(μ-oxo)Cu^{III}Cu^{III} species orbital #107 is vacant while orbital #106 is fully occupied with two electrons. Therefore, the reactivity of the mixed-valent bis(μ-oxo)Cu^{II}-Cu^{III} species is considered to be higher than that of the bis(μ-oxo)Cu^{III}Cu^{III} species, and the former is more favorable for the activation of C−H bonds. Although the reactivity of the bis-(μ-oxo)Cu^{III}Cu^{III} species has been well characterized using synthetic model compounds,[13−15] their oxygenation ability to inert alkanes is not significant in general. Thus, we think that the mixed-valent bis(μ-oxo)Cu^{II}Cu^{III} species is a possible mediator for the conversion of methane to methanol if methane hydroxylation takes place in the dicopper site of pMMO. Although we assumed here that the mixed-valent bis(μ-oxo)-Cu^{II}Cu^{III} species is formed from an initial dicopper^{I} state, it is also possible to consider that it can derive from electron transfer to a bis(μ-oxo)Cu^{III}Cu^{III} species. Chan and co-workers[2,15] reported that the reactivity of bis(μ-oxo)Cu^{III}Cu^{III} can be enhanced upon a one-electron reduction to form a mixed-valent bis(μ-oxo)Cu^{II}Cu^{III} state. This report is fully consistent with our proposal based on the orbital interaction analysis. Injection of an additional electron into bis(μ-oxo)Cu^{III}Cu^{III} produces a σ* SOMO just like orbital #107 (in Figure 6), which plays a crucial role in the homolytic cleavage of a C−H bond of alkanes.

Kinetic Isotope Effects. Having described the reaction pathways and their energetics for methane hydroxylation, we next address the kinetic isotope effects (k_H/k_D) for the H-atom abstraction from methane,[38] which can be calculated from vibrational analyses with transition state theory[31] with Wigner's quantum tunneling correction.[32] The k_H/k_D value is an important measure in discussing how H-atom abstraction from a hydrocarbon substrate takes place in catalytic and enzymatic reactions. The values of k_H/k_D were obtained from the following equation:

$$\frac{k_H}{k_D} = \left(\frac{m_D^R\, m_H^\#}{m_H^R\, m_D^{\#\#}}\right)^{3/2} \left(\frac{I_{xD}^R\, I_{yD}^R\, I_{zD}^R}{I_{xH}^R\, I_{yH}^R\, I_{zH}^R}\right)^{1/2} \left(\frac{I_{xH}^\#\, I_{yH}^\#\, I_{zH}^\#}{I_{xD}^\#\, I_{yD}^\#\, I_{zD}^\#}\right)^{1/2} \frac{q_{\nu D}^R}{q_{\nu H}^R} \frac{q_{\nu H}^R}{q_{\nu D}^\#} \exp\left(-\frac{E_H^\# - E_D^\#}{RT}\right) \quad (1)$$

(38) Yoshizawa, K.; Yumura, T. *Chem. Eur. J.* **2003**, *9*, 2347.

Table 1. Computed KIE (k_H/k_D) Values[a] in the C−H (C−D) Bond Dissociation of Methane by the Mononuclear Model

T (K)	CH_4/CD_4	CH_4/CD_3H	CH_4/CD_2H_2	CH_4/CDH_3
200	33.1 (53.7)	27.4 (44.2)	22.9 (36.7)	19.4 (30.8)
225	24.5 (38.6)	20.4 (30.9)	17.1 (26.6)	14.5 (22.3)
250	19.1 (29.3)	15.6 (24.3)	13.4 (20.4)	11.4 (17.2)
275	15.5 (23.1)	13.0 (19.3)	11.0 (16.2)	9.4 (13.8)
300	12.9 (18.7)	10.9 (15.8)	9.3 (13.4)	8.0 (11.4)
325	11.0 (15.6)	9.3 (13.2)	8.0 (11.2)	6.9 (9.7)
350	9.5 (13.2)	8.1 (11.2)	7.0 (9.7)	6.1 (8.4)
375	8.3 (11.3)	7.2 (9.7)	6.3 (8.4)	5.5 (7.4)
400	7.4 (9.9)	6.5 (8.5)	5.7 (7.5)	5.0 (6.5)

[a] The values in parentheses are KIE values with inclusion of quantum tunneling effects.

Table 2. Computed KIE (k_H/k_D) Values[a] in the C−H (C−D) Bond Dissociation of Methane by the Binuclear Model

T (K)	CH_4/CD_4	CH_4/CD_3H	CH_4/CD_2H_2	CH_4/CDH_3
200	31.0 (46.9)	24.1 (36.2)	18.7 (27.9)	15.0 (22.1)
225	23.3 (34.2)	18.2 (26.5)	14.3 (20.7)	11.5 (16.5)
250	18.3 (26.2)	14.5 (20.5)	11.5 (16.1)	9.3 (13.0)
275	15.0 (20.8)	11.9 (16.5)	9.5 (13.1)	7.8 (10.7)
300	12.5 (17.0)	10.1 (13.6)	8.2 (10.9)	6.8 (9.0)
325	10.7 (14.2)	8.7 (11.5)	7.1 (9.4)	6.0 (7.8)
350	9.3 (12.1)	7.7 (9.9)	6.4 (8.1)	5.4 (6.9)
375	8.2 (10.4)	6.8 (8.6)	5.7 (7.2)	4.9 (6.1)
400	7.3 (9.1)	6.1 (7.6)	5.1 (6.4)	4.5 (5.5)

[a] The values in parentheses are KIE values with inclusion of quantum tunneling effects.

where superscripts R and # specify the reactant methane and the transition state, respectively, for the molecular mass *m*, the moment of inertia *I*, the vibrational partition function *q*, and the activation energy *E*. The last exponential term is dominant in this equation because the other terms can be almost all canceled between the denominators and numerators. The numerator in the last exponential term comes from the fact that C−H dissociation has a lower activation energy than C−D dissociation on account of the former's greater zero-point vibrational energy.

Tables 1 and 2 summarize calculated values of k_H/k_D for the H-atom abstraction via **TS1(m)** of the monocopper species and **TS1(d)** of the dicopper species, respectively, as a function of temperature. Here we adopted CD_4, CD_3H, CD_2H_2, and CDH_3 as deuterium-substituted forms of methane. The coefficient of quantum tunneling correction is written in the form of $\kappa = 1 - 1/24\ (h\upsilon^{\ddagger}/RT)^2$, where $\upsilon^{\ddagger}$ is the imaginary frequency with respect to the transition state for the H-atom abstraction. When the imaginary frequency is large, the potential barrier is thin, and as a result the quantum tunneling effect is significant. The KIE values with Wigner's tunneling correction can be calculated from the expression of $\kappa_H k_H/\kappa_D k_D$.

We list in Table 1 computed KIE values for the H/D-atom abstraction via **TS1(m)** in the monocopper species. The values in parentheses include Wigner's tunneling correction. As expected from the form of eq 1, the KIE values decrease as temperature increases, and at the same time they depend on how many atoms are substituted by deuterium. At 300 K, the KIE for H/D-atom abstraction from CH_4/CD_4 is computed to be 12.9 (18.7) on the basis of transition state theory (with Wigner's tunneling correction) while the one from CH_4/CDH_3 is 8.0 (11.4). The values are about 1.5 times larger when we take the tunneling effect into account. The KIE values decrease as the number of deuterium atoms involved in substrate methane decreases because the vibrational frequencies significantly decrease when the number of deuterium atoms involved is large.

Computed KIE values via **TS1(d)** in the dicopper species are similar to those via **TS1(m)** in the monocopper species, as shown in Table 2, because the transition-state structures are similar with respect to the C−H−O moieties. These values are fully consistent with computed KIE values by a bis(μ-oxo)-Fe^{IV}_2 model of intermediate *Q* of sMMO.[38] At 300 K, the KIE for H-/D-atom abstraction from CH_4/CD_4 is computed to be 12.5 (17.0), while the one from CH_4/CDH_3 is 6.8 (9.0). KIE measurements using [1-$^3H_1$,$^2H_1$] and [1-$^3H_1$,$^2H_1$, 2-$^2H_3$] ethanes as substrates gave values of 5.2 ± 0.4 and 5.5 ± 0.7, respectively.[39] Agreement between these experimental values and the calculated values from CH_4/CDH_3 is fairly good, but the experimental ones are small compared to the calculated ones in general. Although this difference cannot clearly be explained from the theoretical point of view at present, we should note that the calculated KIE values listed in Tables 1 and 2 depend on the number of deuterium atoms. For example, the KIE values for CH_4/CD_4 and those for CH_4/CDH_3 are very different, as mentioned above. This is because KIE values strongly depend on the leading exponential term of eq 1, in which the vibrational structures of molecules as a whole are important rather than the local C−H(D) stretching motion.

Formation of the Copper−Oxo Species. Having described the reactivity of the copper−oxo species, let us next look at the formation of the highly reactive monocopper−oxo species in the protein environment. This species is unstable with respect to dissociation energy,[36c] and how it is formed under physiological conditions is a current interest. The participation of a tyrosine residue in the catalytic mechanism of dopamine β-monooxygenase has been proposed by Klinman and coworkers.[40] In this mechanism, tyrosine is a mediator for the reductive activation of Cu^{II}−OOH to generate a copper−oxo species, which is responsible for the H-atom abstraction from the benzylic position of dopamine. On the basis of this proposal, we can develop a discussion on the formation of the mononuclear Cu^{III}−oxo species of pMMO. Actually Tyr50 and Tyr330 are located 7.6 and 8.0 Å apart, respectively, from the monocopper site of pMMO.[8] We assume that dioxygen is incorporated into the Cu^{I} species in the initial stages of dioxygen activation to give a Cu^{II}−superoxo species, followed by an H-atom transfer from a tyrosine residue near the monocopper active site. A resultant Cu^{II}−hydroperoxo species is next transformed into a Cu^{III}−oxo species and a water molecule by the abstraction of an H-atom from another tyrosine residue. Although this is one possible mechanism for the formation of the Cu^{III}−oxo species from the available crystal structure of pMMO, it is useful to consider the energetics for the formation of the unstable Cu^{III}−oxo species in the protein environment. We calculated the energetics for the formation of the monocopper−oxo species along the line that the two tyrosine residues play a role as providers of H atoms.

Figure 7 shows a computed energy diagram for the formation of the monocopper−oxo species starting from the Cu^{I} species.

(39) Wilkinson, B.; Zhu, M.; Priestley, N. D.; Nguyen, H.-H. T.; Morimoto, H.; Williams, P. G.; Chan, S. I.; Floss, H. G. *J. Am. Chem. Soc.* **1996**, *118*, 921.

(40) (a) Tian, G.; Berry, J. A.; Klinman, J. P. *Biochemistry* **1994**, *33*, 226. (b) Francois, W. A.; Blackburn, N. J.; Klinman, J. P. *Biochemistry* **2003**, *42*, 1813.

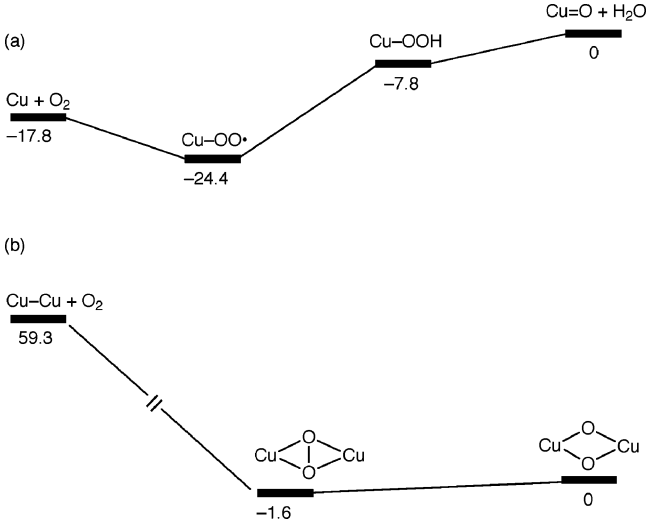

Figure 7. Computed energetics for the formation of the (a) monocopper− and (b) dicopper−oxo species. Unites in kcal/mol.

We roughly estimated the formation energy from the reactions, $Cu-OO^{\bullet} + C_6H_5OH \rightarrow Cu-OOH + C_6H_5O^{\bullet}$ and $Cu-OOH + C_6H_5OH \rightarrow Cu{=}O + H_2O + C_6H_5O^{\bullet}$. The formed phenoxy radicals should be stabilized in energy in the protein environment, whereas the bare phenoxy radicals are not stabilized in the model calculations. As a result, this energetics should be reduced in the protein environment. The formation of the monocopper−oxo species is computed to be 17.8 kcal/mol endothermic. Although the Cu−O bond is weak and this species is unstable in energy, this computed activation energy tells us that this process is accessible under physiological conditions. We next consider the energetics for the formation of the dicopper−oxo species, assuming that dioxygen is initially incorporated into the dicopper site to form a (μ-η^2:η^2-peroxo)-dicopper species, which is then transformed into a bis(μ-oxo)-$Cu^{II}Cu^{III}$ species. Figure 7 also shows a computed energy diagram for the formation of the bis(μ-oxo)$Cu^{II}Cu^{III}$ species, which is computed to be 59.3 kcal/mol exothermic. The reactivity of the bis(μ-oxo)$Cu^{II}Cu^{III}$ species to methane is similar to that of the monocopper−oxo species because the reactivity of these species derives from the antibonding σ* orbitals with respect to the Cu−O bonds of both the monocopper and dicopper reactive species. However, in contrast to the monocopper−oxo species, the formation of the bis(μ-oxo)$Cu^{II}Cu^{III}$ species is downhill in energy, and therefore this process is energetically more favorable than the formation of the monocopper−oxo species.

To look at the reactivity of the mononuclear Cu^{II}−superoxo and Cu^{II}−hydroperoxo species (shown in Figure 7) to methane, we performed additional DFT calculations at the B3LYP* level of theory. A computed activation energy for the H-atom abstraction from methane by the Cu^{II}−superoxo species is 37.0 kcal/mol. Although this species is reported to abstract a benzylic H atom of dopamine,[41] we conclude that it is unable to activate methane under physiological conditions. The Cu^{II}−hydroperoxo species also has no reactivity to methane. Since the reactivity of the Cu^{II}−hydroperoxo species is so weak and at the same time the C−H bonds of methane are so strong that the Cu^{II}−hydroperoxo species cannot abstract an H atom from methane, the reaction intermediate (Cu^{III}−oxo + H_2O + $^{\bullet}CH_3$) that is formed after the C−H cleavage is automatically converted to (Cu^{III}−oxo + $HO^{\bullet}$ + CH_4). This result is fully consistent with previous reports on the poor reactivity of Cu^{II}−hydroperoxo species to dopamine[37,41] and of Fe^{II}−hydroperoxo species to olefins.[42,43]

Conclusions

We have considered the mechanism of methane hydroxylation at the mononuclear and dinuclear copper sites of pMMO using quantum mechanical and QM/MM calculations. If mononuclear and dinuclear copper−oxo species are formed in the enzyme, these species are active enough for converting methane to methanol under physiological conditions. We propose possible mechanisms with respect to how these reactive species are formed. Dioxygen is incorporated into the Cu^{I} species in the initial stages of dioxygen activation to give a Cu^{II}−superoxo species, followed by an H-atom transfer from a tyrosine residue near the monocopper active site. A resultant Cu^{II}−hydroperoxo species is next transformed into a Cu^{III}−oxo species and a water molecule by the abstraction of an H-atom from another tyrosine residue. Since this process was computed to be 17.8 kcal/mol endothermic, the formation of the Cu^{III}−oxo species is possible under physiological conditions. Dioxygen is also incorporated into the dicopper site to form a (μ-η^2:η^2-peroxo)dicopper species, which is then transformed into a bis(μ-oxo)$Cu^{II}Cu^{III}$ species. The formation of this species was computed to be 59.3 kcal/mol exothermic; therefore, this process is more favorable than the formation of the monocopper−oxo species in energy. Detailed DFT calculations demonstrated that the reactivity of the Cu^{III}−oxo species is sufficient for the conversion of methane to methanol, which is 52.9 kcal/mol exothermic relative to the Cu^{III}−oxo species + methane and 35.1 kcal/mol exothermic measured from the initial state of Cu^{I} + O_2. The σ* orbital localized in the Cu−O bond region is singly occupied in the triplet state; therefore, this orbital plays a crucial role in the homolytic cleavage of a C−H bond of methane. The reactivity of the bis(μ-oxo)$Cu^{II}Cu^{III}$ species is also sufficient for the conversion of methane to methanol. This process is 49.2 kcal/mol exothermic relative to that of the bis(μ-oxo)$Cu^{II}Cu^{III}$ species + methane and 110.1 kcal/mol measured from the initial state of the dicopper species + O_2. The reactivity of the mixed-valent bis(μ-oxo)$Cu^{II}Cu^{III}$ species is higher than that of the bis(μ-oxo)-$Cu^{III}Cu^{III}$ species in general because in the former species the amplitude of the σ* SOMO localized on the bridging oxo moieties plays an essential role in the homolytic C−H cleavage. Methyl radical is trapped to the mononuclear and dinuclear copper sites to form intermediates that involve OH and CH_3 ligands. Recombination of the resultant OH and CH_3 ligands takes place in a nonradical manner at a metal active center to form a final methanol complex. These mechanistic proposals are consistent with a nonradical mechanism for the hydroxylation of methane by the diiron active species of sMMO.[44] We finally calculated using transition state theory the kinetic isotope effects for the H-atom abstraction by the Cu^{III}−oxo and

(41) Chen, P.; Solomon, E. I. *J. Am. Chem. Soc.* **2004**, *126*, 4991.
(42) (a) Kamachi, T.; Shiota, Y.; Ohta, T.; Yoshizawa, K. *Bull. Chem. Soc. Jpn.* **2003**, *76*, 721. (b) Kamachi, T.; Shestakov, A. F.; Yoshizawa, K. *J. Am. Chem. Soc.* **2004**, *126*, 3672.
(43) (a) Ogliaro, F.; de Visser, S. P.; Cohen, S.; Sharma, P. K.; Shaik, S. *J. Am. Chem. Soc.* **2002**, *124*, 2806. (b) Sharma, P. K.; Kevorkiants, R.; de Visser, S. P.; Kumar, D.; Shaik, S. *Angew. Chem., Int. Ed.* **2004**, *43*, 1129.
(44) Yoshizawa, K. *Acc. Chem. Res.* **2006**, *39*, 375−382.

bis(μ-oxo)$Cu^{II}Cu^{III}$ species. The value with quantum tunneling correction for CH_4/CD_4 at 300 K is 18.7 for the mononuclear species and 17.0 for the dicopper species.

Acknowledgment. K.Y. acknowledges Grants-in-Aid (No. 18350088 and 18GS02070005) for Scientific Research from Japan Society for the Promotion of Science, the Nanotechnology Support Project of the Ministry of Culture, Sports, Science and Technology of Japan (MEXT), the Joint Project of Chemical Synthesis Core Research Institutions of MEXT, and CREST of Japan Science and Technology Cooperation for their support of this work.

Supporting Information Available: Full author list for ref 23; optimized QM/MM geometries. This material is available free of charge via the Internet at http://pubs.acs.org.

JA061604R